Alloying and dealloying in pulsed laser deposited Pd films on Cu(100)

H. L. Meyerheim,* E. Soyka, and J. Kirschner
Max-Planck-Institut für Mikrostrukturphysik Weinberg 2, D-06120 Halle, Germany
(Received 11 December 2005; revised manuscript received 2 June 2006; published 10 August 2006)

Using surface x-ray diffraction we have studied the geometric structure of ultrathin Pd films grown on Cu(001) at room temperature by pulsed laser deposition in the coverage regime between 0.4 and about 4 monolayers (ML). Up to about 2 ML, the interface formation is characterized by an alloying-dealloying mechanism, where Pd atoms are incorporated into the Cu substrate for less than half-filled layers, but expelled if the Pd coverage is close to a complete layer. In this case the top layer is composed of Pd. Above 2 ML, Pd agglomeration sets in characterized by Pd-rich alloy layers covered by Pd layers. Interlayer spacings linearly depend on the Pd concentration (x) in the Pd_xCu_{1-x} alloy layers in agreement with continuum elasticity considerations. Our results have important implications for modeling strain relaxation.

DOI: 10.1103/PhysRevB.74.085405 PACS number(s): 68.55.−a, 68.35.Ct, 68.47.De, 81.15.Fg

I. INTRODUCTION

During the last decades much work has focused on the investigation of the physics governing the growth, structure, and physical properties of heteroepitaxial films (see, e.g., Refs. 1–6). In all these studies the lattice mismatch (m) between film (f) and substrate (s) is a decisive parameter, which is defined as $m=(a_s-a_f)/a_s$. The lattice mismatch greatly contributes to the interface energy, which contains the specific chemical interactions and the strain energy.[2–5] Due to the fundamental importance of the interface structure an abundance of studies to characterize the structure and properties of heteroepitaxial systems have been carried out thus far. In most experiments the film is prepared by thermal deposition (TD), where the film material is evaporated from a heated rod and recondensed on the substrate crystal.

On the other hand, pulsed laser deposition (PLD) has become an important tool for film preparation. Two aspects of PLD are important for growth, structure, and morphology of the deposited films: (i) an extremely high instantaneous flux of atoms and (ii) the high kinetic energy of the deposited particles. As a rule of thumb a *differential* deposition rate of the order of about 10^6 monolayers (ML)/s can be achieved. Second, the kinetic energy of the deposited particles is estimated to lie in the eV range.[7–9] Despite these potentially advantageous properties, only a few studies have been carried out to prepare ultrathin metallic films, although earlier investigations have shown that metals can be grown by PLD with high quality.[10–12] A review is given by Shen *et al.*[7]

For instance, scanning tunneling microscopy (STM) revealed an improved layer-by-layer growth of PLD-grown Fe on Cu(100) and Cu(111) and a quantitative low-energy-electron diffraction (LEED) analysis indicated a number of subtle structural differences as compared to thermally deposited Fe. These could be related to the different magnetic properties of the differently prepared films.[8,13,14]

Apart from improved layer-by-layer growth, which is related to the high differential deposition rate, interface mixing can occur due to the high kinetic energy of the arriving atoms. In a recent surface x-ray diffraction (SXRD) study on Co/Cu(001) alloy formation was observed for films grown by PLD only, while an epitaxial fcc-like Co overlayer was found for TD.[15]

In this context it is note worthy that interface alloying is an often observed phenomenon for thermally deposited films also, even in cases where no bulk alloy phases exist.[16] Prominent examples are alloys formed by Bi, Mn, Pb, and Pd when deposited at room temperature (RT) on Cu(001) and Cu(111).[17–40]

For bulk Pd_xCu_{1-x} alloys, ordered structures (e.g., of the $L1_2$ type) are only known for low Pd concentrations ($x \leqslant 25-50\%$) and elevated temperatures,[41] but for Pd/Cu(100) two ordered surface alloy phases exist, namely, a c-(2×2) and a $p4gm$-$p(2\times2)$ superstructure corresponding to $\theta=0.5$ and 1 ML coverage, respectively.[28,35,36] In the following we refer to $\theta=1$ ML as 1.53×10^{15}atoms/cm^2, i.e., one adsorbate atom per substrate atom. In the c-(2×2) structure, every other surface Cu atom is substituted by Pd. For the $p4gm$-$p(2\times2)$ structure, evidence has been given that it is composed of two $c(2\times2)$ alloy layers, while the $p4gm$ plane symmetry is induced by a clock rotation of the outermost alloy layer.[35,36]

There exists only one recent report on Pd films grown on Cu(001) by PLD.[42] The evolution of the structure with increasing Pd coverage was studied using STM, LEED, and reflection high-energy electron diffraction (RHEED). Based on STM images and the kinematic interpretation of LEED reflections, layer-by-layer growth of Pd on Cu(001) *without intermixing* was proposed. In combination with experiments on Cu deposited on Pd(001) and molecular dynamics calculations an asymmetry between compressive [Pd/Cu(001)] and tensile [Cu/Pd(001)] stress was inferred, which was related to the asymmetry of the interatomic interactions.

However, the interpretation of the data in terms of a continuous strain relief was based on the assumption that a homogeneous Pd film grows in a layer-by-layer mode, thus excluding any intermixing. In view of the fact that thermally deposited Pd forms an alloy with Cu(001) even at room temperature and that in Ref. 42 the absence of intermixing was concluded from the absence of the $c(2\times2)$ superstructure, this assumption may be questioned.

Therefore, in order to obtain a conclusive picture of the Pd/Cu(001) interface structure prepared by PLD, we have carried out a thorough SXRD study probing the interface evolution in the range between 0.4 and 4 ML. We provide

evidence that Pd growth on Cu(001) is characterized by an alloying-dealloying mechanism up to about 2 ML coverage until Pd agglomeration sets in. Moreover, depending on the Pd concentration within the alloy layers, the interlayer spacings are inhomogeneous within the interfacial regime following predictions based on continuum elasticity theory.

II. EXPERIMENT

The experiments were carried out *in situ* in an ultrahigh-vacuum (UHV) chamber (base pressure: 5×10^{-11} mbar) equipped with a *Z*-axis diffractometer setup for the SXRD data collection.[43] The Cu(001) crystal was cleaned by standard methods (Ar^+-ion sputtering followed by annealing at 900 K) until no traces of contaminants could be observed by Auger-electron spectroscopy (AES). For PLD, a KrF excimer laser (248 nm wavelength, 34 ns pulse length, repetition rate 5 Hz, pulse energy ≈325 mJ) was focused on a Pd target about 120 mm away from the sample surface. Using these parameters an average deposition rate of about 2 ML per minute was achieved. In all cases the sample was kept at room temperature during deposition. The amount of Pd deposited was calibrated by AES using the peak-to-peak intensity rations between the Pd *MNN* and the Cu *LMM* lines and *a posteriori* compared with the Pd coverage derived from the SXRD analysis. The latter provides the total number of ML as the sum of the Pd concentrations over all alloy layers (see below). In general, we find agreement to within 0.2 ML, which is about the uncertainty of the coverage determination for both SXRD and AES.

X rays were generated by a rotating anode system and monochromatized (Cu-$K\alpha$ radiation) by using multilayer optics yielding a peak count rate of several hundred counts/s at the (1 0 0.05) reflection position, close to the (100)-antiphase condition along the (10ℓ) crystal truncation (CTR) rod.[44–47] This is the most surface sensitive position along the CTR. The quantitative evaluation shows that the integrated intensity reflected from the (flat) clean sample is equivalent to the scattering intensity of 0.25 ML.[45]

In order to optimize the count rate, the vertical incoming beam slits were opened to 4 mm, i.e., about 50% of the sample surface (diameter ≈8 mm) is illuminated by the primary beam. In front of the detector, Soller slits are used with an in-plane and out-of-plane resolution of 1.0° and 0.8°, respectively. The first is related to a longitudinal resolution of 0.027 reciprocal lattice units (rlu) at the (1 0 0.1) reflection (1 rlu=1/2.56 Å=0.39 $Å^{-1}$).[47]

Integrated x-ray reflection intensities were collected under total reflection conditions of the incoming beam (incidence angle $\alpha_i\approx0.32°$) by rotating the sample about its surface normal, corresponding to transverse scans over the rod cross section.[44,46]

Figure 1 shows the (1 0 0.1) CTR reflections after deposition of 0.4, 2, and 4 ML Pd. The intensity decreases with increasing Pd coverage, which qualitatively can be interpreted as due to increasing roughness. Moreover, there is no evidence for any lateral relaxation of the peak position within the experimental accuracy of about 0.5% of the Brillouin zone. Due to the limited resolution no attempt was made to analyze possible changes of the beam profiles, but direct inspection of the reflection profiles does not indicate considerable changes with coverage.

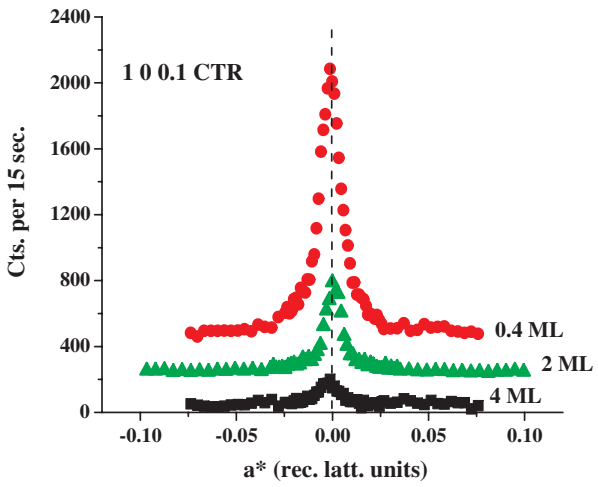

FIG. 1. (Color online) Scans along the a^* direction over the (1 0 0.1) crystal truncation rod reflections after deposition of 0.4 (top), 2 (center), and 4 ML (bottom) Pd. Reflections are on the same scale but shifted for clarity.

The structure factor amplitudes $|F|$ were derived from the integrated intensities after correcting the data for geometric factors.[48] In total, five different data sets corresponding to Pd coverages of 0.4, 1.0, 1.4, 2.0, and 4.0 ML were collected. For each data set four symmetry-independent CTRs [(10ℓ), (11ℓ), (20ℓ), and (21ℓ)] were measured corresponding to about 120 reflections.

As representative examples, symbols in Figs. 2 and 3 show on a logarithmic-scale the $|F|$'s along the (10ℓ), (11ℓ), (20ℓ), and (21ℓ) CTRs for 0.4 and 2.0 ML, respectively.[47] The CTRs were measured up to the maximum momentum transfer of $q_z=1.85$ rlu. It is defined by $q_z=\ell\times c^\star$, where $c^\star=0.28$ $Å^{-1}$ is the rlu of Cu along the surface normal. Note that due to the truncation of the crystal the coordinate of the normal momentum transfer (ℓ) is a continuous parameter.[49]

Because of the high site symmetry (4*mm*) of the atomic positions within the unit cell [(x,y) is either (0,0) or $(\frac{1}{2},\frac{1}{2})$], the (10ℓ) and the (21ℓ) as well as the (11ℓ) and the (20ℓ) rods have the same in-plane phase factor $\exp[i2\pi(hx+ky)]$. For this reason the two rods belonging to each pair exhibit the same overall shape along q_z, although they differ on an absolute intensity scale.

The standard deviations (σ) of the $|F|$'s as represented by the error bars were derived from the counting statistics and the reproducibility of symmetry-equivalent reflections. For each data set two pairs of symmetry equivalent rods were collected, namely, (10ℓ) and (01ℓ) as well as (11ℓ) and $(1\bar{1}\ell)$. In general, (σ) lies in the 5% range, which is an excellent value.

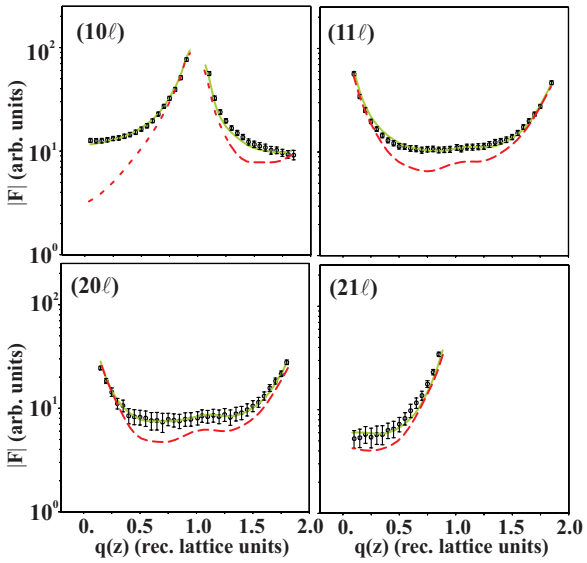

FIG. 2. (Color online) Measured (symbols) and calculated (lines) structure factor amplitudes along the (10ℓ), (11ℓ), (20ℓ), and (21ℓ) CTRs for 0.4 ML Pd/Cu(001). The solid (green) and dashed (red) curves correspond to fits with and without alloy formation. For details see text.

III. STRUCTURE ANALYSIS

A. Evolution of the interface structure

The quantitative structure analysis was carried out by least-squares refinement of the calculated $|F|$'s to the experimental ones.

As outlined in Sec. II, the high symmetry of the structure implies that there is only one independent atomic position per layer located either at (0,0) or at $(\frac{1}{2},\frac{1}{2})$ within the two-dimensional unit cell. Therefore, apart from an overall scale factor only one z parameter and one Debye parameter (B) have to be refined for each layer. Different alloy compositions are represented by the Pd- and Cu-site occupancy factors (θ_{Pd}, θ_{Cu}) with the condition $\theta_{\mathrm{Pd}}+\theta_{\mathrm{Cu}}=1$ in the case of complete layers. Thus, in total only about 10–15 parameters are needed for modeling the structure. In relation to the number of data points (≈120 along four symmetry-independent rods) this is a number low enough to ensure a sufficient overdetermination of the refinement problem. In addition, the correlation between the structure parameters also represents an important factor in the fit procedure. In the present analysis correlations are reasonably low with maximum values in the 0.7–0.8 range, allowing a rapid convergence of the simultaneously fitted parameters.

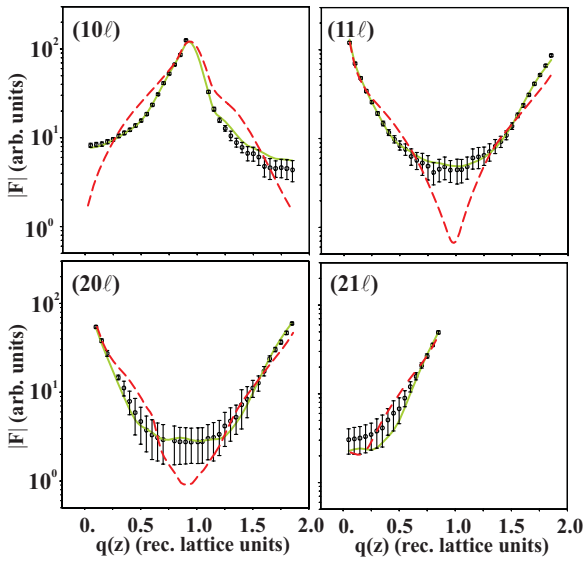

FIG. 3. (Color online) Measured (symbols) and calculated (lines) structure factor amplitudes along the (10ℓ), (11ℓ), (20ℓ), and (21ℓ) CTRs for 2 ML Pd/Cu(001). The lines have the same meaning as in Fig. 2.

Excellent fits could be achieved, which is already evident from visual inspection of the solid (green) lines in Figs. 2 and 3. Similar fit qualities were also obtained for the other data sets. The fit quality is measured by the unweighted residuum (R_u) and by the (statistically more significant) goodness of fit parameter (GOF).[50] These lie in the range of 0.05–0.09 (R_u) and 1.0–1.4 (GOF), indicating nearly perfect agreement between data and fit and suggesting that the results of the structure analysis are highly reliable.

Figure 4 summarizes the evolution of the Pd/Cu(001) interface structure derived from the least-squares refinement. Dark (pink) and bright (grey) bars schematically represent the layer-resolved Pd and Cu concentrations. The stoichiometry is given on the left, where the subscripts indicate the Pd and Cu concentrations in percent of 1 ML. The error bar for the concentration determination is about 5–10 % for each layer. In the following we summarize the results.

In contrast to the interpretation of the STM experiments of Lu *et al.*,[42] we do not find layer-by-layer growth, since the evolution of the interface structure is characterized by an alloying-dealloying process, the latter involving an interlayer exchange between Pd and Cu atoms. Only if one disregards the nature of the surface atoms (as seen by the STM) does the growth look as such, since the alloyed layers tend to exhibit a flat surface.

In general, deposition of Pd on Cu(001) leads to the formation of $\mathrm{Pd}_x\mathrm{Cu}_{1-x}$ alloy layers. In the coverage regime below 2 ML the Pd concentration in the alloys is not observed to exceed 50% [Figs. 4(a)–4(d)]. The only exception represents the topmost layer, which consists of almost pure Pd when one layer is completed (1 ML, 2 ML). We relate this to dealloying when the Pd concentration approaches a "critical" concentration, which we tentatively estimate to about 50%. This is also the maximum Pd concentration found in the ordered superstructures for thermally grown samples and in ordered bulk alloys.[29,35,41] The dealloying mechanism is deduced from the evolution of the interface structure. In detail, during growth of the first layer, deposited Pd atoms form an alloy with Cu, where expelled Cu atoms from islands on top of the alloy [Fig. 4(a)]. When the first layer is complete [Fig. 4(b)], the topmost layer is Pd rich (due to some overdosing, some Cu is found above the Pd layer). We suggest that when the Pd concentration in the alloy exceeds about 50% an interlayer exchange process takes place, where Pd atoms from the alloy are expelled to the topmost layer and Cu atoms from the topmost-layer islands are reincorporated into the

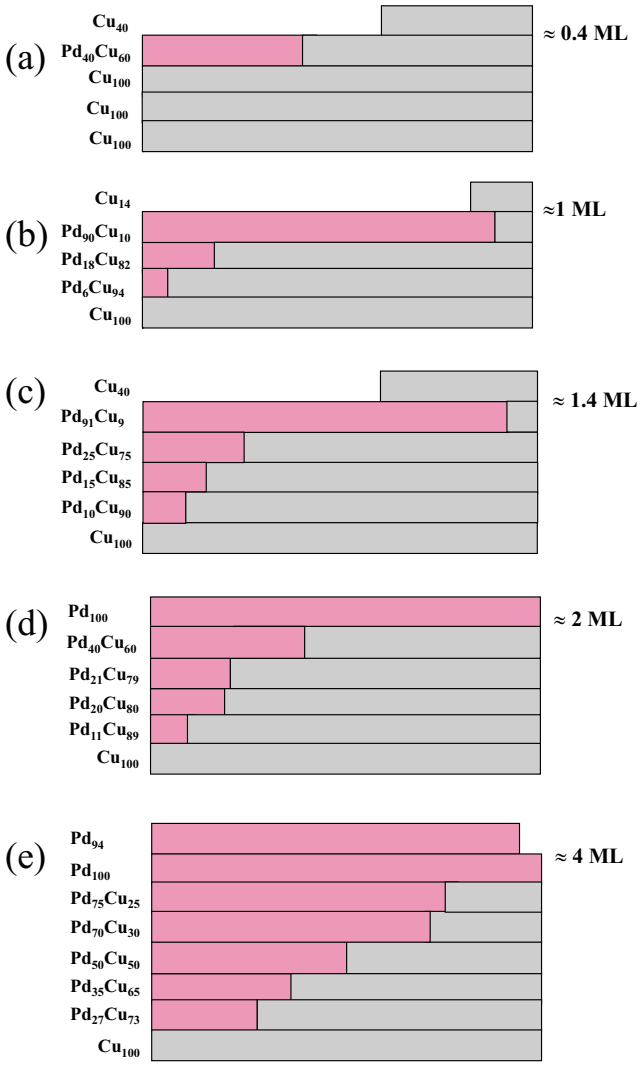

FIG. 4. (Color online) Layer resolved alloy concentrations for about 0.4 (a), 1 (b), 1.4 (c) 2 (d), and 4 (e) ML Pd on Cu(001). Dark (pink) and bright (grey) bars schematically represent the Pd and Cu concentrations in the layers. Labels on the left indicate the layer stoichiometry.

second layer. Similarly, proceeding with the growth of the second layer, Cu islands are found on the surface, while the Pd concentration in the deeper layers increases [Fig. 4(c)], but when the second layer is complete, the surface consists of (almost) pure Pd [Fig. 4(d)]. Simultaneously, an interface roughness develops. In this respect the PLD-prepared interface bears some resemblance to TD-prepared Pd/Cu(111), where a disordered CuPd alloy is formed extending over several layers.[39]

At higher coverage [≈4 ML, Fig. 4(e)] three alloy layers are observed characterized by Pd concentrations in the 50–70% range. On top of these alloy layers we find two layers of pure Pd. Simultaneously STM images show the formation of misfit dislocation lines.[42]

On the basis of these structure models very good fits are achieved, but in order to prove the sensitivity of the SXRD data to distinguish between structural models involving or excluding alloying, we have also carried out calculations assuming pure Pd layers on Cu(001) as claimed in Ref. 42.

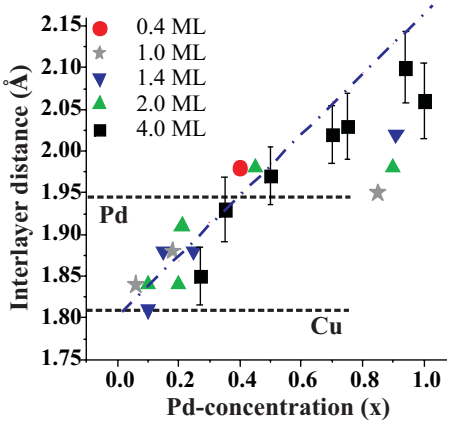

FIG. 5. (Color online) Interlayer spacings versus Pd concentration (x) in Pd_xCu_{1-x} alloy layers. Symbols refer to different coverages as indicated. Horizontal lines correspond to the bulk Cu (1.808 Å) and Pd (1.945 Å) interlayer spacings. The (blue) dash-dotted line represents the calculated layer spacings based on continuum elasticity theory. Error bars are indicated for the 4 ML sample only.

The dotted (red) lines in Figs. 2 and 3 represent the calculated $|F|$'s for 0.4 and 2.0 ML Pd on Cu(001). It is directly evident that the calculated $|F|$'s strongly deviate from the experimental ones, especially close to the antiphase scattering conditions, where the surface sensitivity is at its maximum. For the nonalloy models we obtain for R_u and GOF values in the range of 0.2–0.3 and 4.0, respectively. These are about four times larger than those for the best fit and clearly show that models assuming Pd growth on Cu(001) without intermixing can be discarded.

Qualitatively, the increased steepness of the calculated intensity distribution along the rods for the nonalloy models is related to stronger electron density contrast as compared to the alloyed one. In summary, the SXRD analysis allows a clear distinction between the alloy and nonalloy structure models. This is due to the considerable difference between the atomic scattering amplitudes of Pd and Cu, resulting from the difference of the atomic number ($Z_{Cu}=29$, $Z_{Pd}=46$; note that the scattered intensity is proportional to Z^2).

B. Interlayer spacings

The SXRD analysis also provides more subtle details on the atomic interface structure. The interlayer spacings (d_{ij}) between adjacent layers (i) and (j) show an almost linear dependence on the Pd concentration in the alloy layers. In Fig. 5 the d_{ij}'s are plotted versus Pd concentration (x). Different symbols refer to samples covered by 0.4 up to 4 ML as indicated. Error bars for the distance determination lie in the 0.03–0.05 Å range as shown for the 4 ML sample (solid squares).

For low Pd concentrations, the interlayer spacings are very close to that of bulk Cu (1.808 Å), while with increasing (x) the d_{ij}'s continuously increase and pass the bulk Pd value (1.945 Å) for $x \approx 0.45$. For $x > 0.5$, the interlayer spac-

ings continue to increase and approach values in the 2.05–2.10 Å range.

The dependence of d_{ij} on the Pd concentration can be analyzed on the basis of continuum elasticity theory taking into account the dependence of the alloy's equilibrium lattice constant on the Pd concentration. Linde[51] has investigated the lattice parameters of bulk (disordered) fcc Pd_xCu_{1-x} solid solutions over the whole concentration range. There is a nearly linear dependence of the lattice constant on the Pd concentration,[52] sometimes referred to as "Vegard's law." In consequence, the misfit (m) of the alloy layers to the given substrate lattice linearly depends on the Pd concentration.

Considering the bulk lattice constants of Cu (2.556 Å) and Pd (2.751 Å),[47] Pd grows on Cu(001) under compressive strain with a lateral misfit of $\varepsilon_1=\varepsilon_2=-0.072$. Using Poisson's ratio for Pd ($\nu=0.44$),[53] and the equation $\varepsilon_3/(\varepsilon_1+\varepsilon_2)=-\nu/(1-\nu)$, one finds $\varepsilon_3=+0.11$, i.e., the normal lattice spacing of Pd is calculated to increase by 11%. Consequently, if pure Pd is grown pseudomorphically on Cu, continuum elasticity predicts an interlayer spacing of 2.16 Å, but smaller expansions are calculated for alloy layers with decreasing (x) as shown by the (blue) dashed line in Fig. 5. It represents the calculated interlayer spacing taking into account the interpolated equilibrium lattice parameters of the Pd_xCu_{1-x} alloys.

It should be emphasized that this approach needs a caveat for two reasons. First, nothing is known about the elastic constants of either, ultrathin Pd films or Pd_xCu_{1-x} alloys. Thus, in view of the lack of a more appropriate description, we refer to the available bulk data. This approach might seem to be of limited validity; however, recent work on monolayer strain clearly indicates that continuum elasticity does provide a meaningful estimate of theoretical lattice spacings, even in the monolayer regime.[54,55]

Second, hydrogen adsorption from the residual gas atmosphere is known to lead to an expansion of the Pd interlayer spacings.[56] Some influence of hydrogen on the interlayer spacings cannot be excluded in the present case at least for layers of very high Pd concentration. Correcting for the hydrogen effect would lead to slightly lower d_{ij}'s, but preserving the overall dependency of d_{ij} on (x).

As shown in Fig. 5, the experimental interlayer spacings well match the calculated ones; some deviations are observed for Pd concentrations above about 60–70 % only. This might be related to the breakdown of the model assumption of homogeneously strained layers. The STM images of Lu *et al.*[42] showing the onset of misfit dislocations lines at a coverage of 4 ML support this view. Another indication for an increasing structural disorder with increasing Pd coverage comes from the analysis of the static disorder which is outlined in the following.

C. Disorder

Structural disorder as expressed by the Debye parameter (B) was refined for each layer simultaneously. In the most general case, B describes the displacement of an atom out of its average position, which can be dynamic (thermal vibrations) or static (average over an ensemble of displaced atoms) in nature. In the case of isotropic displacements, the mean square displacement of an atom out of its average position, $\langle u^2\rangle$, is related to B by the relation $B=8\pi^2\langle u^2\rangle$. Taking into account anisotropic displacement amplitudes according to the condition imposed by the 4*mm* point group symmetry of the atomic sites ($\langle u_{11}^2\rangle=\langle u_{22}^2\rangle\neq\langle u_{33}^2\rangle$) did not lead to better fits, most likely due to the limited k-space access.

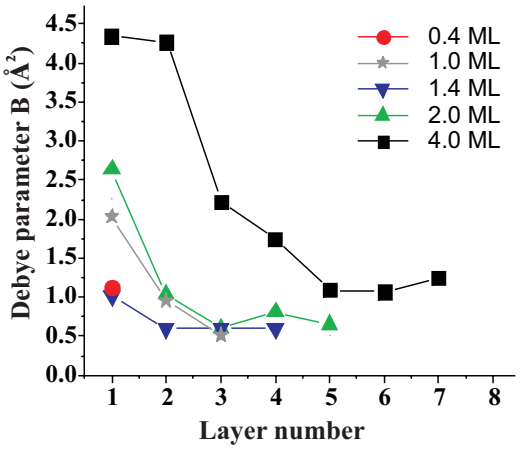

FIG. 6. (Color online) Layer-resolved Debye parameters for Pd on Cu(001). Layers are numbered from the top (layer 1) to the interior of the crystal. Only B factors for alloyed layers are shown. Lines are guides to the eye.

Figure 6 shows the isotropic layer-resolved B's for all samples. Layers are numbered from the top (layer 1) to the interior of the crystal. Only the alloyed layers are considered; the B factors of deeper layers rapidly converge to the bulk (room temperature) value of $B=0.6$ Å^2.[57] Standard deviations calculated from the variance-covariance matrix are in the range of 10–30 %, which for SXRD data is an excellent value.

In the near-surface region, disorder significantly increases, which goes in parallel with the increasing Pd concentration. Without temperature-dependent measurements it is not possible to separate the thermal disorder from the static one, but B parameters in the 2–5 Å^2 range corresponding to root mean square displacement amplitudes ($\sqrt{\langle u\rangle^2}$) between 0.16 and 0.25 Å cannot be attributed to thermal vibrations only. They rather represent static disorder due to incorporation of the large Pd atoms in the alloy layers and—most evident for the 4 ML sample—due to structural relaxation related to the emergence of dislocation lines.

IV. DISCUSSION

The SXRD analysis provides a conclusive and consistent picture of the Pd/Cu(001) interface formation. As far as the growth mode (layer by layer) and the surface morphology is concerned our experiments are in good agreement with the RHEED and STM results presented in Ref. 42, but they provide clear evidence that the interface structure is inhomogeneous with respect to the Pd concentration and with respect to the interlayer distances. The latter show an almost linear dependence on the Pd concentration following predictions based on continuum elasticity.

We have developed a model where the interface formation can be roughly separated into two regimes, a first one up to about 2 ML, where alloying-dealloying processes take place, and a second one, where Pd agglomeration at the surface begins, coinciding with the observation of misfit dislocation lines.

In general, surface alloying by a metal species whose atomic radius is larger than that of the substrate can be understood by considering that bare surfaces are under tensile stress[58,59] and that incorporation of larger atoms is a mechanism to gain surface energy γ_S.[60,61] As pointed out by Harrison,[61] the equilibrium structure is determined by the total energy minimization and not only by the gain in surface energy, which represents only one contribution to the total energy. Therefore, other contributions must be taken into account, such as adsorbate-substrate hybridization and charge transfer. In this context surface alloying might be favored since it increases the adsorbate's coordination number.

So far, for the Pd/Cu system experimental[17,18,23–29,33–35,39,40,62] and theoretical work[34,36,63,64] has been carried out, focusing on the the mechanisms of alloy formation and segregation, but quantitative structure analyses were carried out for TD-deposited films only. For the (001)-, (110)-, and (111)-oriented Cu-substrate surface, alloying was determined, but ordered structures were found for the (001) and (110) surface only.

Since for TD, surface alloying is observed, PLD should also lead to alloy formation. This is because of the higher kinetic energy of the deposited atoms of the order of a few eV, which is sufficient to overcome the kinetic barrier of interdiffusion.[9] Only a few quantitative structure analyses exist comparing the interface structures prepared by TD and PLD.[14,15] In the most recent study on room-temperature-deposited Co on Pd(001) a face-centered tetragonal Co overlayer forms in the case of TD, but extensive alloying occurs in the case of PLD. *Ab initio* calculations revealed that the activation energy (E_a) for alloying equals 0.4 eV/atom,[15] large enough to hinder interdiffusion in the TD case at room temperature, but not in the case of PLD.

The observation that for TD-grown Pd/Cu(001) formation of the c-(2×2) structure already starts at 170 K implies that the activation energy (E_a) for alloying is even lower than for Co/Pd(001). Pope *et al.*[21] have investigated in detail the kinetics of the alloy formation. For the initial stage of the alloy formation they derived $E_a=0.34\pm0.02$ eV/atom, some 15% lower than calculated for Co/Pd(001) and—at least qualitatively—in correspondence with the low temperature alloying. In conclusion, alloy formation in PLD-grown Pd/Cu(001) is expected and in agreement with our results.

As outlined in Fig. 4(a) surface alloying proceeds in the same way as reported in a previous STM study[28] characterized by growth of Cu islands above the alloyed layer. It should be emphasized that on the basis of the CTR data it is not possible to determine whether or not the Cu islands grow above Pd_xCu_{1-x} alloy islands or not. This is because the analysis of the integer-order CTRs projects (and averages) the structure into the (1×1) unit cell.

In contrast to the case of TD preparation, the c-(2×2) superstructure was not observed for PLD (see also Ref. 42). In order to explain this phenomenon, it is tempting to speculate that the high deposition energy in PLD might lead to a structure characterized by randomly distributed patches of (1×1)-ordered alloyed Pd islands, since even the presence of many small c-(2×2)-like alloyed islands separated by antiphase domains would lead to a c-(2×2) diffraction pattern. Due to the larger atomic radius of Pd as compared to Cu (1.36 versus 1.28 Å) for this configuration a large strain energy is expected to pile up locally, likely inducing some atomic relaxation. Indication for structural relaxation is provided by the considerably enhanced Debye parameters (see Fig. 6) observed for all samples in the near-surface regime. Similar arguments also apply for the nonalloyed Pd overlayers, where the Pd atoms are located in the hollow sites of the underlying PdCu alloy. The B factors of these layers are also strongly enhanced.

Extrapolation of the growth process to the completion of the first ML would lead to a Cu/Pd/Cu(001) sandwich, locally resembling the CuAu alloy ($L1_0$) structure, but this is not observed. Instead, a restructuring takes place involving a dealloying process leading to an almost pure Pd top layer and a Cu-rich Pd_xCu_{1-x} alloy underneath. With increasing Pd concentration strain energy piles up and—at a certain critical concentration—the dealloying process sets in.

Dealloying processes are quite common and numerous systems are known, e.g., Au/Ni(110),[65] Pb/Cu(111),[20] Bi/Cu(001),[30] Pb/Cu(100),[32] Mn/Cu(001),[38] and Bi/Cu(111).[37] Although the structures of the alloyed phases and the mechanisms of dealloying differ in detail, relief of strain energy is the driving force for dealloying in general.

The alloying-dealloying process continues during growth of the second monolayer [Figs. 4(c) and 4(d)], but increasing the Pd coverage beyond 2 ML leads to the enrichment of Pd at the surface [Fig. 4(e)]. We suggest that at this coverage the restructuring of the interface becomes diffusion limited, since for coverages beyond 1 ML the interlayer site exchange becomes more complex by involving multiple site exchange processes characterized by a considerably increased E_a. Quantitative estimates of E_a for the present system are not known, but for comparison we refer to the study of Goapper,[66] who found a bulk ordering activation energy of 2.2 eV in the $Pd_{17}Cu_{83}$ alloy, which is in the same range as the kinetic energy of the deposited atoms. With increasing Pd coverage a diffusion barrier continuously builds up, leading to a Pd concentration gradient in the alloy structure and to a rough interface (alloyed) structure between the bulk Cu and the Pd overlayer.

Finally, the strain energy is released by formation of misfit dislocations implying lateral relaxations. Increased static disorder is evidenced by the strongly enhanced B factors for the top Pd layers in the 4 ML sample and represents an (indirect) indication for the appearance of this morphological feature observed in STM. Quantitatively, the largest value observed for the top layer, $B=4.3$ Å^2, corresponds to a root mean square displacement amplitude of 0.23 Å representing the radius of the displacement sphere. Correspondingly, the peak-to-peak displacement amplitude equals 0.46 Å, in reasonable agreement with the height of 0.57 Å of the protrusions observed in STM.[42]

V. SUMMARY

We have presented a quantitative SXRD study of the evolution of the interface structure for Pd grown on Cu(001) by PLD. In contrast to the previous simplistic model based on the interpretation of STM and RHEED claiming layer-by-layer growth of Pd excluding intermixing, we find a complicated growth mechanism characterized by alloying, dealloying, and Pd agglomeration above an alloyed structure. The interface structure is inhomogeneous with respect to both Pd concentration of the alloy layers and the interlayer spacings. The latter show an almost linear dependence on the Pd concentration within the alloy layers, which can be explained by continuum elasticity considerations. Our study may have important implications for state of the art calculations modeling the strain relief mechanisms in Pd-Cu heteroepitaxy.

ACKNOWLEDGMENT

The authors would like to thank W. Greie for technical assistance.

*Electronic address: hmeyerhm@mpi-halle.mpg.de

[1] E. Bauer, Z. Kristallogr. **110**, 372 (1958).
[2] E. Bauer and J. H. van der Merwe, Phys. Rev. B **33**, 3657 (1986).
[3] R. Kern, G. Lelay, and J. J. Métois, Curr. Top. Mater. Sci. **3**, 145 (1978).
[4] R. Kern, in *Interfacial Aspects in Phase Transformations*, Proceedings of the Advanced NATO Study Institute, edited by B. Mutaftschiev (Reidel, Dordrecht, 1981), p. 287.
[5] P. Müller and R. Kern, Appl. Surf. Sci. **102**, 6 (1996).
[6] P. Müller and R. Kern, Appl. Surf. Sci. **164**, 68 (2000).
[7] J. Shen, Z. Gai, and J. Kirschner, Surf. Sci. Rep. **52**, 163 (2004).
[8] J. Shen, P. Ohresser, Ch. V. Mohan, M. Klaua, J. Barthel, and J. Kirschner, Phys. Rev. Lett. **80**, 1980 (1998).
[9] S. Fähler and H. U. Krebs, Appl. Surf. Sci. **96–98**, 1980 (1998).
[10] H. Schwartz and H. A Tourtellotte, J. Vac. Sci. Technol. **6**, 373 (1969).
[11] Y. A. Bykowski, V. M. Boyakov, V. T. Galochkin, A. S. Molchanov, I. N. Nikolayev, and A. N. Oraevski, Sov. Phys. Tech. Phys. **23**, 578 (1978).
[12] O. F. K. McGrath, F. Robaut, N. Cherief, A. Lienard, M. Brunel, and D. Givord, Surf. Sci. **315**, 218 (1998).
[13] H. Jenniches, J. Shen, Ch. V. Mohan, S. S. Manoharan, J. Barthel, P. Ohresser, M. Klaua, and J. Kirschner, Phys. Rev. B **59**, 1196 (1999).
[14] M. Weinelt, S. Schwarz, H. Baier, S. Müller, L. Hammer, K. Heinz, and Th. Fauster, Phys. Rev. B **63**, 205413 (2001).
[15] H. L. Meyerheim, V. Stepanyuk, A. L. Klavsyuk, E. Soyka, and J. Kirschner, Phys. Rev. B **72**, 113403 (2005).
[16] J. Tersoff, Phys. Rev. Lett. **74**, 434 (1995).
[17] G. W. Graham, Surf. Sci. **171**, L432 (1986).
[18] S. C. Wu, S. H. Lu, Z. Q. Wang, C. K. C. Lok, J. Quinn, Y. S. Li, D. Tian, F. Jona, and P. M. Marcus, Phys. Rev. B **38**, 5363 (1988).
[19] M. Wuttig, Y. Gauthier, and S. Blügel, Phys. Rev. Lett. **70**, 3619 (1992).
[20] C. Nagl, O. Haller, E. Platzgummer, M. Schmid, and P. Varga, Surf. Sci. **321**, 237 (1994).
[21] T. D. Pope, K. Griffiths, V. P. Zhdanov, and P. R. Norton, Phys. Rev. B **50**, 18553 (1994).
[22] R. G. P. van der Kraan and H. van Kempen, Surf. Sci. **338**, 19 (1995).
[23] J. Yao, Y. G. Shen, D. J. O'Connor, and B. V. King, J. Vac. Sci. Technol. A **13**, 1443 (1995).
[24] P. W. Murray, I. Stensgaard, E. Lægsgaard, and F. Besenbacher, Phys. Rev. B **52**, R14404 (1995).
[25] T. D. Pope, M. Vos, H. T. Tang, K. Griffith, I. V. Mitchell, P. R. Norton, W. Liu, Y. S. Li, K. A. R. Mitchell, Z.-J. Tian, and J. E. Black, Surf. Sci. **337**, 79 (1995).
[26] Y. G. Shen, J. Yao, D. J. O' Connor, B. V. King, and R. J. MacDonald, Solid State Commun. **100**, 21 (1996).
[27] J. Yao, Y. G. Shen, D. J. O'Connor, and B. V. King, Surf. Sci. **359**, 65 (1996).
[28] P. W. Murray, I. Stensgaard, E. Lægsgaard, and F. Besenbacher, Surf. Sci. **365**, 591 (1996).
[29] Y. G. Shen, A. Bilić, D. J. O'Connor, and B. V. King, Surf. Sci. **394**, L131 (1997).
[30] H. L. Meyerheim, H. Zajonz, W. Moritz, and I. K. Robinson, Surf. Sci. **381**, L551 (1997).
[31] H. L. Meyerheim, M. De Santis, W. Moritz, and I. K. Robinson, Surf. Sci. **418**, 295 (1998).
[32] R. Plass and G. L. Kellog, Surf. Sci. **470**, 106 (2000).
[33] C. J. Barnes, E. AlShamaileh, T. Pitkänen, P. Kauksoina, and M. Lindroos, Surf. Sci. **492**, 55 (2001).
[34] M. L. Grant, B. S. Swartzentruber, N. C. Bartelt, and J. B. Hannon, Phys. Rev. Lett. **86**, 4588 (2001).
[35] K. Pussi, M. Lindroos, E. ALShamaileh, and C. J. Barnes, Surf. Sci. **513**, 555 (2002).
[36] D. Spisak and J. Hafner, Phys. Rev. B **67**, 235403 (2003).
[37] D. Kaminski, P. Poodt, E. Aret, N. Radenovic, and E. Vlieg, Surf. Sci. **575**, 233 (2005).
[38] W. Pan, R. Popescu, H. L. Meyerheim, D. Sander, O. Robach, S. Ferrer, M.-T. Lin, and J. Kirschner, Phys. Rev. B **71**, 174439 (2005).
[39] A. Siervo, E. A. Soares, R. Landers, T. A. Fazan, J. Morais, and G. G. Kleinman, Surf. Sci. **504**, 215 (2002).
[40] A. Canzian, H. O. Mosca, and G. Bozzolo, Surf. Sci. **551**, 9 (2004).
[41] P. R. Submaranian and D. E. Laughlin, in *Binary Alloy Phase Diagrams*, edited by T. B. Massalski (ASM International, Metals Park, OH, 1990), Vol. 2.
[42] Y. Lu, M. Przybylski, O. Tushin, W. H. Wang, J. Barthel, E. Granato, S. C. Ying, and T. Ala-Nissila, Phys. Rev. Lett. **94**, 146105 (2005).
[43] M. Bloch, J. Appl. Crystallogr. **18**, 33 (1985).
[44] R. Feidenhans'l, Surf. Sci. Rep. **10**, 105 (1989).
[45] I. K. Robinson, in *Handboook of Synchrotron Radiation*, edited by G. S. Brown and D. E. Moncton (Elsevier, Amsterdem, 1991), Vol. 3.
[46] I. K. Robinson and D. J. Tweet, Rep. Prog. Phys. **55**, 599 (1992).
[47] The surface (s) setting is related to the fcc setting of the bulk (b) by the following relations: $[100]_s=(1/2)([100]_b-[010]_b)$,

$[010]_s=(1/2)([100]_b+[010]_b)$, and $[001]_s=[001]_b$.

[48] E. Vlieg, J. Appl. Crystallogr. **30**, 532 (1997).

[49] I. K. Robinson, Phys. Rev. B **33**, 3830 (1986).

[50] R_u is defined as $R_u=\Sigma||F_{obs}|-|F_{calc}||/\Sigma|F_{obs}|$, where F_{obs} and F_{calc} are the observed and calculated structure factors, respectively, and the summation runs over all data points. The goodness of fit (GOF) is defined as $\sqrt{\left[\frac{1}{(N-P)}\right]\Sigma w(|F_{obs}|-|F_{calc}|)^2}$, where N and P are the numbers of reflections and refined parameters, respectively, and $w=1/\sigma^2$ is the weighting factor using the standard deviation (σ) as parameter.

[51] J. O. Linde, Ann. Phys. **15**, 249 (1932).

[52] W. B. Pearson, *Lattice Spacings and Structures of Metals and Alloys* (Pergamon Press, London, 1964).

[53] R. F. S. Hearmon, in *The Elastic Constants of Crystals and Other Anisotropic Materials*, edited by K.-H. Hellwege and A. M. Hellwege, Landolt-Börnstein, New Series, Group III, Vol. 18, supplement to III/IV (Springer, Berlin, 1984).

[54] D. Sander, W. Pan, S. Ouazi, J. Kirschner, W. Meyer, M. Krause, S. Müller, L. Hammer, and K. Heinz, Phys. Rev. Lett. **93**, 247203 (2004).

[55] E. Groppo, C. Prestipino, C. Lamberti, P. Luches, C. Giovanardi, and F. Boscherini, J. Phys. Chem. B **107**, 4597 (2003).

[56] S. H. Kim, H. L. Meyerheim, J. Barthel, J. Kirschner, J. Seo, and J.-S. Kim, Phys. Rev. B **71**, 205418 (2005).

[57] *International Tables for Crystallography*, edited by C. H. MacGillavry and G. D. Rieck (Kluwer Academic, Dordrecht, 1985), Vol. 3.

[58] H. Ibach, Surf. Sci. Rep. **29**, 195 (1997).

[59] D. Sander, Rep. Prog. Phys. **62**, 809 (1999).

[60] D. P. Woodruff and E. Vlieg, in *Surface Alloys and Alloy Surfaces*, edited by D. P. Woodruff (Elsevier, Amsterdam, 2002), Vol. 10, p. 277.

[61] M. J. Harrison, D. P. Woodruff, and J. Robinson, Surf. Sci. **572**, 309 (2004).

[62] P. W. Murray, S. Thorshaug, I. Stensgaard, F. Besenbacher, E. Lægsgaard, A. V. Ruban, K. W. Jacobson, G. Kopidakis, and H. L. Skriver, Phys. Rev. B **55**, 1380 (1997).

[63] C. Gallis, B. Legrand, and G. Treglia, Surf. Rev. Lett. **4**, 1119 (1997).

[64] G. Treglia, B. Legrand, F. Ducastelle, A. Saul, C. Gallis, I. Meuner, C. Mottet, and A. Senhaji, Comput. Mater. Sci. **15**, 196 (1999).

[65] L. P. Nielsen, F. Besenbacher, I. Stensgaard, E. Lægsgaard, C. Engdahl, P. Stoltze, and J. K. Nørskov, Phys. Rev. Lett. **74**, 1159 (1995).

[66] S. Goapper, L. Barbier, B. Salanon, A. Loiseau, and X. Torrelles, Phys. Rev. B **57**, 12497 (1998).